Coordination of the potentially tridentate ligands 2,6-diacetylpyridinebis(anil) (dapa) and 2-(2-(2′-methylidenepyridyl)aminoethyl)pyridine (map) in the complexes *fac*-$BrMn(CO)_3L$, *fac*-$(CO)_5MM'(CO)_3L$ (M, M′ = Mn, Re; L = dapa, map) and their photoproducts. The crystal structure of $BrMn(CO)_2$(N,N,N-dapa)

G.J. Stor, M. van der Vis, D.J. Stufkens and A. Oskam

Anorganisch Chemisch Laboratorium, Universiteit van Amsterdam, Nieuwe Achtergracht 166, 1018 WV Amsterdam (Netherlands)

J. Fraanje and K. Goubitz

Laboratorium voor Kristallografie, Universiteit van Amsterdam, Nieuwe Achtergracht 166, 1018 WV Amsterdam (Netherlands)

(Received November 17, 1993)

Abstract

In complexes of the type *fac*-$(CO)_5MM'(CO)_3$(N,N-L) (M, M′ = Mn, Re; L = dapa, map) the potentially tridentate ligand L is bidentately (N,N) coordinated to the metal centre M′. Irradiation of these complexes into their lowest-energy absorption band resulted in metal–metal bond homolysis and/or loss of CO from the $M'(CO)_3$(N,N-L) fragment.

Upon irradiation of *fac*-$(CO)_5MRe(CO)_3$(N,N-dapa) (M = Mn, Re) only the metal–metal bond homolysis reaction was observed. The 16-electron $Re^+(CO)_3$(N,N-dapa$^-$) species thus formed was readily converted into the 18-electron radical complex $Re^+(CO)_3$(N,N,N-dapa$^-$) by coordination of the third nitrogen donor atom of dapa to the Re centre, as shown by ESR spectroscopy. Addition of excess PR_3 (R = nBu, Ph) gave rise to the immediate conversion of $Re^+(CO)_3$(N,N,N-dapa$^-$) into the $Re^+(CO)_3$(N,N-dapa$^-$)(PR_3) adduct.

The tendency of the dapa ligand to adopt a tridentate coordination mode was also reflected in the ready formation of the complexes $BrMn(CO)_2$(N,N,N-dapa) and $(CO)_5ReMn(CO)_2$(N,N,N-dapa). The X-ray structure of the former complex was determined; the dapa ligand is coordinated in-plane and the CO ligands are in a mutually *cis*-disposition.

Irradiation of *fac*-$(CO)_5MMn(CO)_3$(N,N-map) (M = Mn, Re) at low temperature gave the CO-bridged complex $(CO)_4M(\mu$-$CO)Mn(CO)_2$(N,N-map). In the absence of CO, the latter complex reacted thermally to give $(CO)_5MMn(CO)_2$(N,N,N-map). For M = Mn this complex was stable only below 263 K, whereas for M = Re it was obtained as a stable photoproduct at room temperature. Metal–metal bond homolysis of *fac*-$(CO)_5ReRe(CO)_3$(N,N-map) at temperatures below 203 K was followed by a recombination of the resulting $\cdot Re(CO)_5$ and $Re^+(CO)_3$(N,N-map$^-$) radicals, which was accompanied by a change in coordination of the map ligand.

Key words: Manganese, Rhenium; Carbonyls; Photochemistry; Crystal structure; Diimine

1. Introduction

Complexes of the type *fac*-$(CO)_5MM'(CO)_3(\alpha$-diimine) (M, M′ = Mn, Re; α-diimine = bpy, phen, *etc.*) have been found to undergo metal–metal bond homolysis and/or release of CO from the $M'(CO)_3(\alpha$-diimine) fragment upon irradiation into their visible absorption band [1]. Which type of reaction took place depended on M and M′ in the sense that release of CO only occurred for complexes with M′ = Mn. When the complexes *fac*-$(CO)_5MnMn(CO)_3(\alpha$-diimine) were irradiated in the presence of an excess of PR_3 or another nucleophile, a photocatalytic disproportionation reaction was observed, which was initiated by the radical complexes $Mn^+(CO)_3(\alpha$-diimine$^-$)(PR_3) [1d,f].

Correspondence to: Prof. D.J. Stufkens.

0022-328X/94/$7.00
SSDI 0022-328X(94)24602-F

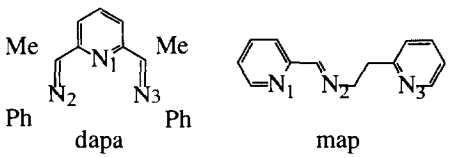

Fig. 1. Structures of the ligands dapa and map with atom labeling.

These radical complexes were also found to initiate the catalytic substitution of CO by PR_3 in $M_3(CO)_{12}$ (M = Fe, Ru) to give $M_3(CO)_{11}(PR_3)$ [1f].

Since these electron transfer chain reactions can only occur when the 16-electron $Mn^+(CO)_3(\alpha\text{-diimine}^-)$ radicals are stabilized by adduct formation with a nucleophile such as PR_3, this nucleophile must always be present in excess in the solution. As a result, only those reactions can be studied in which PR_3 is a reactant or which are not influenced at all by this ligand. It seemed possible that this restriction might be removed by using an α-diimine with a coordinating side-arm instead of the free nucleophile PR_3. With this in mind we have synthesized a new series of complexes, *viz.* *fac*-$(CO)_5MM'(CO)_3$(N,N-L) (M, M' = Mn, Re), in which L denotes one of the tridentate ligands of Fig. 1, 2,6-diacetylpyridine-bis(anil) (dapa) and 2-(2-(2'-methylidenepyridyl)aminoethyl)pyridine) (map). Both ligands coordinate to M' via two nitrogen atoms (= N,N). Upon metal–metal bond homolysis the 16-electron radical complex $M'(CO)_3$(N,N-L) can form the coordinatively saturated complex $M'(CO)_3$(N,N,N-L) by adduct formation through the third nitrogen donor atom of the α-diimine ligand L.

This article describes the synthesis, spectroscopic properties and photochemistry of a series of complexes *fac*-$(CO)_5MM'(CO)_3$(N,N-L) (M, M' = Mn, Re; L = dapa, map), where general structure is depicted in Fig. 2.

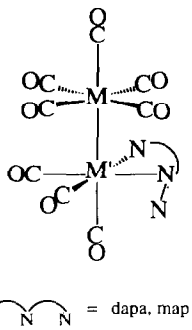

Fig. 2. General molecular geometry of the complexes *fac*-$(CO)_5MM'(CO)_3$(N,N-L).

2. Experimental section

2.1. Materials and preparations

All solvents were distilled from Na under nitrogen. $Re_2(CO)_{10}$, $Mn_2(CO)_{10}$, AgOtf ($Otf^- = CF_3SO_3^-$), tBuNO and PPh_3 were obtained commercially and used without further purification. $P(^nBu)_3$ was distilled under vacuum from CaH_2. The dapa [2] and map [3] were synthesized by standard procedures.

The *fac*-$BrRe(CO)_3$(N,N-dapa) complex was synthesized as previously described [4] except that the solution of the reactants in toluene was refluxed for three hours. The *fac*-$BrRe(CO)_3$(N,N-map) complex was synthesized analogously. *fac*-$BrMn(CO)_3$(N,N-dapa) was synthesized as previously described [4] except that the solution of the reactants in hexane was refluxed for thirty minutes with exclusion of light. *fac*-BrMn $(CO)_3$(N,N-map) was made analogously.

$BrMn(CO)_2$(N,N,N-dapa) was prepared by refluxing a solution of equimolar amounts of $BrMn(CO)_5$ [5] and dapa in hexane for four hours with exclusion of light. The product separated at room temperature as dark purple microcrystals, which were filtered off, washed with hexane, and dried under vacuum; it was obtained in almost quantitative yield.

fac-$(CO)_5MM'(CO)_3$(N,N-L) (M, M' = Mn, Re; L = dapa, map) and $(CO)_5ReMn(CO)_2$(N,N,N-dapa) were synthesized by the method used for the related *fac*-$(CO)_5MM'(CO)_3(\alpha\text{-diimine})$ complexes [6]. In all cases, except for $(CO)_5ReMn(CO)_2$(N,N,N-dapa), the *fac*-$BrM'(CO)_3$(N,N-L) complexes were transformed into *fac*-$M'(CO)_3$(N,N-L)$^+Otf^-$ [7] prior to the reaction with $M(CO)_5^-$. All the dinuclear metal–metal bounded complexes were purified by column chromatography on Silica 60 (activated by heating overnight under vacuum at 150°C) with the exclusion of light with gradient elution by hexane-THF. Yields of 30–60% were obtained.

Elemental analyses were by the Elemental Analysis section of the Institute for Applied Chemistry (TNO), Zeist, The Netherlands.

All spectroscopic samples were made up by use of standard inert gas techniques.

dapa. ^{1}H-NMR (acetone-d_6, 293 K) δ: 8.36 (d, 2H), 8.03 (t, 1H), 7.41 (t, 4H), 7.12 (t, 2H), 6.88 (d, 4H), 2.40 (s, 6H). UV/Vis λ_{max} (THF, 293 K): 330 nm.

map. ^{1}H-NMR (acetone-d_6, 293 K) δ: 8.58 (t, 1H), 8.36 (s, 1H), 8.04 (d, 1H), 7.70 (m, 2H), 7.23 (m, 4H), 4.09 (t, 2H, β-CH_2), 3.17 (t, 2H, α-CH_2).

fac-$BrMn(CO)_3$(N,N-dapa). IR ν(CO) (CH_2Cl_2, 293 K): 2028s, 1943m, 1925m cm^{-1}. UV/Vis λ_{max} (THF, 293 K): 460 nm.

fac-$BrRe(CO)_3$(N,N-dapa). IR ν(CO) (CH_2Cl_2, 293 K): 2026s, 1928m, 1903m cm^{-1}. UV/Vis λ_{max} (THF,

293 K): 420 nm. ^{1}H-NMR (acetone-d_6, 293 K) δ: 8.49 (dd, 2H), 8.14 (t, 1H), 7.45 (m, 6H), 7.18 (m, 4H), 2.60 (s, 3H), 2.54 (s, 3H).

$BrMn(CO)_2$(N,N,N-dapa). IR ν(CO) (CH_2Cl_2, 293 K): 1939s, 1875m cm^{-1}. UV/Vis λ_{max} (THF, 293 K): 540 nm. ^{1}H – NMR (acetone-d_6, 293 K) δ: 8.18 (s br, 3H), 7.31 (m, 10H), 2.37 (s, 6H).

fac-$BrMn(CO)_3$(N,N-map). IR ν(CO) (THF, 293 K): 2020s, 1935m, 1915m cm^{-1}. UV/Vis λ_{max} (THF, 293 K): 455 nm. ^{1}H-NMR (acetone-d_6, 293 K) δ: 9.25 (d, 1H), 8.72 (s, 1H), 8.56 (d, 1H), 8.13 (s br, 2H), 7.72 (t, 2H), 7.32 (m, 2H), 4.69 (t, 2H), 3.58 (t, 2H).

fac-$BrRe(CO)_3$(N,N-map). IR ν(CO) (THF, 293 K): 2020s, 1922m, 1897m cm^{-1}. UV/Vis λ_{max} (THF, 293 K): 420 nm. ^{1}H-NMR ($CDCl_3$, 293 K) δ: 8.98 (d, 1H), 8.62 (s, 1H), 8.55 (d, 1H), 7.87 (m, 2H), 7.52 (t, 2H), 7.26 (m, 2H), 4.67 (t, 2H), 3.52 (t, 2H).

fac-$(CO)_5ReRe(CO)_3$(N,N-dapa). Anal. Found: C, 38.51; H, 2.27; N, 4.56; O, 13.77. Calcd.: C, 38.20; H, 2.10; N. 4.61; O, 14.04%. IR ν(CO) (THF, 293 K): 2076m, 1991vs, 1970m, 1957m, 1947sh, 1902m, 1886m cm^{-1}. UV/Vis λ_{max} (THF, 293 K): 575, 390sh nm. ^{1}H-NMR (acetone-d_6, 293 K) δ: 8.51 (d, 1H), 8.23 (t, 1H), 7.89 (d, 1H), 7.43 (m, 6H), 7.13 (m, 4H), 2.76 (s, 3H), 2.52 (s, 3H).

fac-$(CO)_5MnRe(CO)_3$(N,N-dapa). Anal. Found: C, 44.25; H, 2.79; N, 5.03; O, 15.78. Calcd.: C, 44.64; H, 2.45; N, 5.39; O, 16.24%. IR ν(CO) (THF, 293 K): 2054m, 1997vs, 1956m, 1943m, 1906m, 1897m cm^{-1}. ^{1}H-NMR (acetone-d_6, 293 K) δ: 8.54 (d, 1H), 8.32 (t, 1H), 8.00 (d, 1H), 7.45 (m, 6H), 7.15 (m, 4H), 2.77 (s, 3H), 2.52 (s, 3H).

$(CO)_5ReMn(CO)_2$(N,N,N-dapa). Anal. Found: C, 45.43; H, 2.96; N, 5.59; O, 14.37. Calcd.: C, 44.80; H, 2.55; N, 5.60; O, 14.92%. IR ν(CO) (THF, 293 K): 2071s, 2007w, 1975vs, 1960s, 1946m, 1895s, 1851w cm^{-1}; IR ν(CO) (hexane, 293 K): 2076s, 2016w, 1980vs, 1966s, 1957m, 1908s, 1868w cm^{-1}. UV/Vis λ_{max} (THF, 293 K): 560, 490sh, 375sh nm. ^{1}H-NMR (acetone-d_6, 293 K) δ: 8.43 (d, 2H), 8.14 (t, 1H), 7.15 (m, 10H), 2.73 (s, 6H).

fac-$(CO)_5ReRe(CO)_3$(N,N-map). Anal. Found: C, 31.18; H, 1.74; N, 5.16; O, 15.94. Calcd.: C, 31.23; H, 1.62; N, 5.20; O, 15.85%. IR ν(CO) (THF, 293 K): 2075m, 1990vs, 1968s, br, 1951sh, 1896m, 1891m cm^{-1}. UR/Vis λ_{max} (THF, 293 K): 535, 370sh nm. ^{1}H-NMR (C_6D_6, 293 K) δ: 8.62 (d, 1H), 8.40 (d, 1H), 7.92 (s, 1H), 6.89 (d, 2H), 6.50 (m, 4H), 4.55 (m, 2H), 3.31 (t, 2H).

fac-$(CO)_5ReMn(CO)_3$(N,N-map). Anal. Found: C, 37.19; H, 2.04; N, 6.21; O, 18.70. Calcd.: C, 37.28; H, 1.94; N, 6.21; O, 18.92%. IR ν(CO) (THF, 293 K): 2080m, 2005w, 1979vs, 1966m, 1892m cm^{-1}. UV/Vis λ_{max} (THF, 293 K): 570, 375 nm. ^{1}H-NMR (acetone-d_6, 293 K) δ: 9.22 (d, 1H), 8.73 (s, 1H), 8.56 (d, 1H), 8.13 (d, 1H), 7.89 (t, 1H), 7.67 (d, 1H), 7.33 (m, 3H), 4.71 (t, 2H), 3.55 (m, 2H).

fac-$(CO)_5MnMn(CO)_3$(N,N-map). IR ν(CO) (THF, 293 K): 2056m, 1981vs, 1959s, 1901m cm^{-1}. UV/Vis λ_{max} (THF, 293 K): 565, 355 nm.

2.2. Spectroscopic measurements and photochemistry

IR spectra were recorded on a Nicolet 7199B FTIR interferometer fitted with a liquid-nitrogen cooled MCT detector (32 scans, resolution 1.0 cm^{-1}). Electronic absorption spectra were recorded on a Perkin Elmer Lambda 5 UV/Vis spectrophotometer, equipped with a 3600 data station. Low temperature IR and UV/Vis measurements were performed with an Oxford Instruments DN 1704/54 liquid nitrogen cryostat, equipped with a conventional IR cell or a FAIR cell [8]. ^{1}H-NMR spectra were recorded on Bruker AC 100 or AMX 300 spectrometers and ESR spectra on a Varian E6 spectrometer with 100 kHz modulation.

For irradiation of the spectroscopic samples, use was made of a Spectra Physics 2025 Ar^+ laser, a tunable CR 490 dye laser with Rhodamine 6G as dye, an Oriel 100 W high pressure mercury lamp, and a Philips HPK 125 W high pressure mercury lamp provided with the appropriate interference filter.

Spectroelectrochemical redox reactions were performed *in situ* in an IR spectroelectrochemical Optically Transparent Thin Layer Electrochemical (OTTLE) cell [9], equipped with a Pt-minigrid working electrode (32 wires/cm). The region of the working electrode was masked carefully to avoid the spectral beam passing through the non-electrolyzed solution. Controlled-potential electrolyses within the OTTLE cell were carried out with a PAR Model 174 potentiostat.

For all photochemical and spectroelectrochemical reactions the concentration of the substrate complex was about 10^{-2} M.

2.3. Crystal structure determination of $BrMn(CO)_2$(N,N,N-dapa)

Experimental details for the crystal structure determination of $BrMn(CO)_2$(N,N,N-dapa) are shown in Table 1. A crystal with dimensions ca. $0.25 \times 0.30 \times 0.40$ mm was used for data collection on an Enraf-Nonius CAD-4 diffractometer with graphite-monochromated Cu Kα radiation and ω-2θ scan. A total of 3783 unique reflections was measured within the range $0 \leq h \leq 10$, $0 \leq k \leq 19$, $-17 \leq 1 \leq 17$. Of these, 2823 were above the significance level of 2.5 $\sigma(I)$. The maximum value of $(\sin \theta)/\lambda$ was 0.59 Å^{-1}. Two reference reflections (202, 141) were measured hourly and showed a

TABLE 1. Crystallographic data and refinement details for $BrMn(CO)_2$(N,N,N-dapa)

Chemical formula	$C_{23}H_{19}N_3O_2BrMn$
M_r	504.3
Crystal class	monoclinic
Space group	$P2_1/c$
a/Å	8.9218(8)
b/Å	16.794(1)
c/Å	14.9417(8)
β/deg	95.299(7)
V/Å^3	2229.2(3)
Z	4
D_x/g.cm^{-3}	1.50
λ (Cu Kα)/Å	1.5418
μ (Cu Kα)/cm^{-1}	71.54
F (0,0,0)	1016
T/K	293
R	0.039
R_w	0.057

40% decrease during the 42 h collection time, and a correction was made for this. Unit cell parameters were refined by a least-squares fitting procedure using 23 reflections with $80° \leq 2\theta \leq 85°$. Corrections for Lorentz and polarization effects were applied. The positions of Mn and Br were found by Direct Methods. The remainder of the non-hydrogen atoms were found in a subsequent ΔF synthesis. The hydrogen atoms were placed in calculated positions. Full-matrix least-squares refinement of F, anisotropic for the non-hydrogen atoms and isotropic for the hydrogen atoms, restraining the latter in such a way that the distance to their carrier remained constant at approximately 1.09 Å, converged to $R = 0.039$, $R_w = 0.057$, $(\Delta/\sigma)_{max} = 0.39$. A weighting scheme $w = (10.8 + F_{obs} + 0.0083 \times (F_{obs})^2)^{-1}$ was used. An empirical absorption correction (DIFABS) [10] was applied, with coefficients in the range of 0.54–1.30. A final difference Fourier map revealed a residual electron density between −0.4 and 0.3 eÅ^{-3}. Scattering factors were taken from Cromer and Mann [11]. The anomalous scattering of Mn and Br was taken into account. All calculations were performed with XTAL [12], unless stated otherwise. The fractional coordinates and the equivalent isotropic thermal parameters of the non-hydrogen atoms are given in Table 2. The bond distances and angles for the non-hydrogen atoms are given in Tables 3 and 4, respectively.

3. Results and discussion

The metal–metal bonded complexes *fac*-$(CO)_5$-$MM'(CO)_3$(N,N-L) (M, M′ = Mn, Re; L = dapa, map) were prepared by the well-established reaction (1) between $M(CO)_5^-$ and *fac*-$XM'(CO)_3$(N,N-L) (X = halide) or *fac*-$M'(CO)_3$(N,N-L)$^+$Otf$^-$ [6].

$$M(CO)_5^- + fac\text{-}XM'(CO)_3(N,N\text{-}L) \longrightarrow fac\text{-}(CO)_5MM'(CO)_3(N,N\text{-}L) + X^- \quad (1)$$

TABLE 2. Fractional coordinates and equivalent isotropic thermal parameters for the non-hydrogen atoms of $BrMn(CO)_2$(N,N,N-dapa) with esd's in parentheses

Atom	x	y	z	U_{eq}/Å^2
Br	0.89440(6)	0.56783(3)	0.26429(4)	0.0564(3)
Mn	0.67811(7)	0.63848(4)	0.32932(4)	0.0356(3)
C(1)	0.7881(5)	0.5615(3)	0.4925(3)	0.047(3)
C(2)	0.8114(6)	0.4980(4)	0.5527(3)	0.062(3)
C(3)	0.7329(7)	0.4274(3)	0.5331(4)	0.067(3)
C(4)	0.6355(6)	0.4202(3)	0.4564(4)	0.061(3)
C(5)	0.6167(5)	0.4847(3)	0.3973(3)	0.048(3)
C(6)	0.8604(5)	0.6399(3)	0.4960(3)	0.048(3)
C(7)	0.9688(6)	0.6623(4)	0.5759(3)	0.063(3)
C(8)	0.8785(5)	0.7650(3)	0.4194(3)	0.049(3)
C(9)	0.8217(6)	0.8232(3)	0.4726(4)	0.057(3)
C(10)	0.8602(7)	0.9023(3)	0.4583(4)	0.068(4)
C(11)	0.9528(7)	0.9223(3)	0.3927(4)	0.068(4)
C(12)	1.0088(7)	0.8638(4)	0.3418(4)	0.067(3)
C(13)	0.9715(6)	0.7844(3)	0.3540(3)	0.059(3)
C(14)	0.5238(6)	0.4902(3)	0.3111(3)	0.049(3)
C(15)	0.4309(7)	0.4214(3)	0.2752(4)	0.073(4)
C(16)	0.4479(5)	0.5764(3)	0.1884(3)	0.048(3)
C(17)	0.3010(6)	0.5995(4)	0.1908(4)	0.068(4)
C(18)	0.2221(8)	0.6254(5)	0.1113(5)	0.095(5)
C(19)	0.2905(9)	0.6277(5)	0.0325(5)	0.103(5)
C(20)	0.4360(9)	0.6024(5)	0.0313(4)	0.095(5)
C(21)	0.5177(7)	0.5758(4)	0.1098(3)	0.068(4)
C(22)	0.6852(5)	0.7065(3)	0.2379(3)	0.044(2)
C(23)	0.5279(5)	0.6984(3)	0.3635(3)	0.047(3)
N(1)	0.6906(4)	0.5538(2)	0.4184(2)	0.041(2)
N(2)	0.8247(4)	0.6832(2)	0.4261(2)	0.043(2)
N(3)	0.5375(4)	0.5577(2)	0.2718(2)	0.042(2)
O(22)	0.6874(5)	0.7500(2)	0.1779(2)	0.067(2)
O(23)	0.4329(5)	0.7388(2)	0.3809(3)	0.079(3)

TABLE 3. Bond distances (Å) in $BrMn(CO)_2$(N,N,N-dapa) with esd's in parentheses

Mn–Br	2.5342(9)	C(8)–C(13)	1.379(7)
Mn–C(22)	1.787(4)	C(8)–N(2)	1.462(6)
Mn–C(23)	1.788(5)	C(9)–C(10)	1.394(8)
Mn–N(1)	1.944(4)	C(10)–C(11)	1.380(9)
Mn–N(2)	2.004(4)	C(11)–C(12)	1.365(8)
Mn–N(3)	1.988(4)	C(12)–C(13)	1.390(8)
C(1)–C(2)	1.398(7)	C(14)–C(15)	1.493(7)
C(1)–C(6)	1.464(7)	C(14)–N(3)	1.288(6)
C(1)–N(1)	1.351(5)	C(16)–C(17)	1.370(7)
C(2)–C(3)	1.395(8)	C(16)–C(21)	1.379(7)
C(3)–C(4)	1.378(8)	C(16)–N(3)	1.451(6)
C(4)–C(5)	1.398(7)	C(17)–C(18)	1.39(1)
C(5)–C(14)	1.469(7)	C(18)–C(19)	1.37(1)
C(5)–N(1)	1.356(6)	C(19)–C(20)	1.37(1)
C(6)–C(7)	1.513(7)	C(20)–C(21)	1.395(8)
C(6)–N(2)	1.288(6)	C(22)–O(22)	1.158(6)
C(8)–C(9)	1.384(7)	C(23)–O(23)	1.135(6)

TABLE 4. Bond angles (deg) of $BrMn(CO)_2$(N,N,N-dapa) with esd's in parentheses

Br–Mn–C(22)	85.6(2)	C(2)–C(1)–N(1)	120.0(4)
Br–Mn–C(23)	172.1(2)	C(3)–C(4)–C(5)	119.2(5)
Br–Mn–N(1)	85.5(1)	C(4)–C(5)–C(14)	128.9(4)
Br–Mn–N(2)	89.0(1)	C(4)–C(5)–N(1)	119.3(4)
Br–Mn–N(3)	89.3(1)	C(5)–C(14)–C(15)	121.0(4)
Mn–C(22)–O(22)	178.8(4)	C(5)–C(14)–N(3)	112.7(4)
Mn–C(23)–O(23)	176.2(4)	C(6)–C(1)–N(1)	111.3(4)
Mn–N(1)–C(1)	118.9(3)	C(6)–N(2)–C(8)	121.9(4)
Mn–N(1)–C(5)	118.1(3)	C(7)–C(6)–N(2)	126.3(5)
Mn–N(2)–C(6)	118.0(3)	C(8)–C(9)–C(10)	118.5(5)
Mn–N(2)–C(8)	120.0(3)	C(8)–C(13)–C(12)	119.1(5)
Mn–N(3)–C(14)	119.1(3)	C(9)–C(8)–C(13)	121.1(5)
Mn–N(3)–C(16)	120.0(3)	C(9)–C(8)–N(2)	119.0(4)
C(22)–Mn–C(23)	86.5(2)	C(9)–C(10)–C(11)	120.8(5)
C(22)–Mn–N(1)	170.9(2)	C(10)–C(11)–C(12)	119.7(5)
C(22)–Mn–N(2)	104.2(2)	C(11)–C(12)–C(13)	120.8(5)
C(22)–Mn–N(3)	99.8(2)	C(13)–C(8)–N(2)	119.6(4)
C(23)–Mn–N(1)	102.3(2)	C(14)–C(5)–N(1)	111.9(4)
C(23)–Mn–N(2)	92.2(2)	C(14)–N(3)–C(16)	120.9(4)
C(23)–Mn–N(3)	92.8(2)	C(15)–C(14)–N(3)	126.2(4)
N(1)–Mn–N(2)	77.8(1)	C(16)–C(17)–C(18)	118.4(6)
N(1)–Mn–N(3)	77.9(1)	C(16)–C(21)–C(20)	118.1(6)
N(2)–Mn–N(3)	155.7(1)	C(17)–C(16)–C(21)	122.2(5)
C(1)–C(2)–C(3)	118.2(5)	C(17)–C(16)–N(3)	119.4(5)
C(1)–C(6)–C(7)	119.9(4)	C(17)–C(18)–C(19)	120.6(6)
C(1)–C(6)–N(2)	113.8(4)	C(18)–C(19)–C(20)	120.0(6)
C(1)–N(1)–C(5)	122.4(4)	C(19)–C(20)–C(21)	120.7(6)
C(2)–C(1)–C(6)	128.6(4)	C(21)–C(16)–N(3)	118.3(4)
C(2)–C(3)–C(4)	120.9(5)		

For the complexes *fac*-$XM'(CO)_3$(N,N-L) the bidentate coordination of L in the case of dapa was evident from, for example, the ^{1}H-NMR spectra of *fac*-$BrM'(CO)_3$(N,N-dapa). The spectra showed two sharp methyl proton singlets at 2.59 and 2.55 ppm, respectively, for M' = Mn and 2.60 and 2.54 ppm for M' = Re. The small but clear separation between these singlets indicates that the two imine groups of dapa are inequivalent.

The ^{1}H-NMR spectrum of the free map ligand showed two proton singlets at 4.09 and 3.17 ppm, respectively, which belong to the two CH_2 groups. On the basis of recent reports [3], the triplet at 4.09 ppm can be assigned to the β-CH_2 group (*i.e.* the CH_2 group bonded to the imine-nitrogen atom) and the triplet at 3.17 ppm to the α-CH_2 group (*i.e.* the CH_2 group bonded to the pyridine ring). In the mononuclear *fac*-$BrM'(CO)_3$(N,N-map) complexes the map ligand is most probably coordinated to the metal via the nitrogen atoms N_1 and N_2 (see Fig. 1). The ^{1}H-NMR spectra of both complexes exhibited two triplets at high field arising from the two CH_2 groups of the map ligand.

Attempts to make the metal–metal bonded complexes by use of reaction 1 were unsuccessful in the case of M' = Mn and L = dapa. The complexes *fac*-$XMn(CO)_3$(N,N-dapa) instead underwent reaction 2, even in the presence of only small amounts of $M(CO)_5^-$.

$$\textit{fac}\text{-}XMn(CO)_3(N,N\text{-dapa}) \xrightarrow{M(CO)_5^-} XMn(CO)_2(N,N,N\text{-dapa}) + CO \quad (2)$$

The corresponding map complexes followed reaction 1. Reaction 2 is catalytic and the substitution takes place via an electron transfer chain mechanism. Similar reduction-induced substitutions have been observed by Kochi for a wide range of metal carbonyl complexes [13]. In order to confirm this mechanism, the reaction was also induced by electrochemical reduction of the parent complex in an OTTLE cell. In this way the IR spectral changes during the reduction process could be followed. Again, $BrMn(CO)_2$(N,N,N-dapa) was formed as the only product (reaction 3).

$$\textit{fac}\text{-}BrMn(CO)_3(N,N\text{-dapa}) \xrightarrow{+e^-} BrMn(CO)_2(N,N,N\text{-dapa}) + CO \quad (3)$$

A similar reduction-induced CO-substitution has been observed previously for the complexes $M(CO)_4$(bpy) (M = Cr, Mo, W), which, in the presence of PPh_3, reacted upon one-electron reduction to give $M(CO)_3(bpy)(PPh_3)$ [14].

fac-$BrMn(CO)_3$(N,N-map) could only be converted photochemically into the thermally unstable $BrMn(CO)_2$(N,N,N-map) (ν(CO) in THF: 1920s, 1847m cm^{-1}) by irradiation into its visible absorption band.

Before discussing the photochemistry of the metal–metal bonded complexes of both dapa and map, we briefly describe the spectroscopic and structural properties of the complexes $BrMn(CO)_2$(N,N,N-dapa) and $(CO)_5ReMn(CO)_2$(N,N,N-dapa), in which the dapa ligand is coordinated in tridentate mode to manganese. The photochemistry of the latter complex is discussed together with the photoreactions of the *fac*-$(CO)_5MM'(CO)_3$(N,N-L) (L = dapa, map) complexes.

In contrast to that of *fac*-$BrMn(CO)_3$(N,N-dapa), the ^{1}H-NMR spectrum of $BrMn(CO)_2$(N,N,N-dapa) only shows one singlet at 2.37 ppm for the two methyl groups of the dapa ligand, which points to a tridentate in-plane coordination of the ligand. The corresponding spectrum of $(CO)_5ReMn(CO)_2$(N,N,N-dapa) also showed one singlet at 2.73 ppm.

On going from *fac*-$BrMn(CO)_3$(N,N-dapa) to $BrMn(CO)_2$(N,N,N-dapa) the MLCT band is shifted from 460 to 540 nm and the CO-stretching frequencies from 2028s, 1943m, 1925m to 1942s, 1874m cm^{-1}. These shifts are due to the σ-donor properties of the third nitrogen atom being stronger than those of CO, while the position of the MLCT band is also influenced by the lowering in energy of the lowest π^* orbital

TABLE 5. CO-stretching frequencies of the parent metal–metal bonded complexes and their photoproducts

Complex	Solvent	T [K]	ν(CO) [cm^{-1}]		
fac-$(CO)_5ReRe(CO)_3$(N,N-dapa)	THF	293	2076m	1991vs	1970m
			1957m	1947sh	1902m
			1886m		
fac-$(CO)_5MnRe(CO)_3$(N,N-dapa)	THF	293	2054m	1997vs	1956m
			1943m	1906m	1897m
$(CO)_5ReMn(CO)_2$(N,N,N-dapa)	THF	293	2071s	2007w	1975vs
			1960s	1946m	1895s
			1851w		
fac-$(CO)_5ReRe(CO)_3$(N,N-map)	THF	293	2075m	1990vs	1968s,br
			1951sh	1896m	
			1891m		
fac-$(CO)_5ReMn(CO)_3$(N,N-map)	THF	293	2080m	2005w	1979vs
			1966m	1892m	
fac-$(CO)_5MnMn(CO)_3$(N,N-map)	THF	293	2056m	1981vs	1959s
			1901m		
$FRe(CO)_5$	C_6F_6	293	2152vs	2044vs	2017m
$ClRe(CO)_5$	THF	293	2154vw	2041vs	1980m
$HRe(CO)_5$	THF	293	2011s,br		
	hexane	293	2016vs	2007m	1984vw
$Re_2(CO)_9(P(^nBu)_3)$	THF	203	2102w	2034w	1988vs
			1944w	1925m	
cis-$HRe(CO)_4(P(^nBu)_3)$	THF	293	2074m	1979s	1965vs
			1946m		
mer,trans-$HRe(CO)_3(P(^nBu)_3)_2$	THF	293	1907vs		
fac-$BrRe(CO)_3$(N,N-dapa	THF	293	2028s	1930s	1903s
fac-$BrMn(CO)_3$(N,N-dapa)	CH_2Cl_2	293	2028s	1943m	1925m
$BrMn(CO)_2$(N,N,N-dapa)	THF	293	1942s	1874m	
$Re(CO)_3$(N,N,N-dapa)$^+$	THF	293	2020s	1922s	1901s
	THF	203	2021s	1918s	1898s
	toluene	293	2022s	1929s	1897s
	toluene	203	2024s	1918s	1901s
$Re(CO)_3$(N,N-dapa)(THF)$^+$	THF	203	2033s	1925s	1912s
$Re(CO)_3$(N,N-dapa)(2-MeTHF)$^+$	2-MeTHF	143	2030s	1922s	1913s
$Re(CO)_3$(N,N-dapa)$(PPh_3)^+$	toluene	293	2036s	1954s	1925s
$Re(CO)_3$(N,N-dapa)$(P(^nBu)_3)^+$	THF	203	2031s	1943s	1921s
$Re^+(CO)_3$(N,N-dapa$^-$)(2-MeTHF)	2-MeTHF	143	2008s	1897s	1885s
$Re^+(CO)_3$(N,N-dapa$^-$)(CH_3CN) [a]	CH_3CN	243	2009s	1899s,br	
$Re^+(CO)_3$(dpp$^-$)(THF) [a]	THF	293	2008s	1898s	1881s
$Re^+(CO)_3$(N,N-dapa$^-$)(THF)	THF	203	2008s	1897s	1887
$Re^+(CO)_3$(N,N-dapa$^-$)(PPh_3)	THF	293	2014s	1917s	1895s
$Re^+(CO)_3$(N,N-dapa$^-$)$(P(^nBu)_3)$	THF	293	2010s	1913s	1887s
fac-$ClRe(CO)_3$(N,N-map)	THF	293	2021s	1921s	1897s
fac-$BrMn(CO)_3$(N,N-map)	THF	293	2025s	1938s	1922
$Re^+(CO)_3$(N,N-map$^-$)(PPh_3)	THF	293	2016s	1923s	1890s
$Re^+(CO)_3$(N,N-map$^-$)$(P(^nBu)_3)$	THF	293	2011s	1929s	1884s
$Mn_2(CO)_6$(N,N-map)$_2$	THF	293	1990m	1972w	1947vs
			1897m	1873m	
$(CO)_4Mn(\mu$-CO)$Mn(CO)_2$(N,N-map)	2-MeTHF	133	2041m	1970w	1946vs
			1927m	1878m	1821m
$(CO)_5MnMn(CO)_2$(N,N,N-map)	2-MeTHF	183	2045m	1974w	1947vs
			1930m	1887m	1834m
$Mn_2(CO)_4(\sigma,\sigma,\eta^2$-map)$_2$	THF	203	1971s	1895s,br	
	toluene	203	1972s	1894s,br	
$(CO)_4Re(\mu$-CO)$Mn(CO)_2$(N,N-map)	2-MeTHF	133	2065m	1986w	1965s
			1930m	1863m	1808m
$(CO)_5ReMn(CO)_2$(N,N,N-map)	2-MeTHF	293	2065m	1988w	1965s
			1935m	1877m	1824m
$(CO)_5ReRe(CO)_3(N_2,N_3$-map) [b]	THF	203	2075m	2021vs	1972s
			1966s	1927s	1915s
			1902s		

[a] From ref. 24. [b] Atom labelling according to Fig. 1.

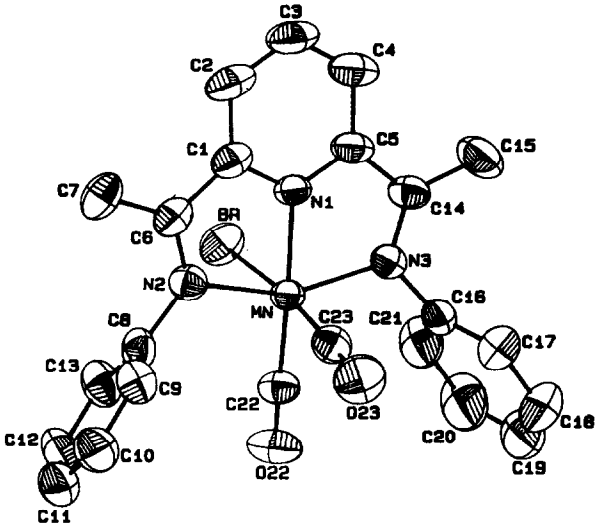

Fig. 3. Crystal structure (ORTEP drawing) of $BrMn(CO)_2(N,N,N\text{-dapa})$.

when the dapa ligand adopts the tridentate in-plane coordination. The complex $(CO)_5ReMn(CO)_2(N,N,N\text{-dapa})$ (ν(CO) see Table 5) has an absorption band at 560 nm with a shoulder at 490 nm. Their positions do not depend on the solvent, which means that the transitions involved have little MLCT character because of the strong metal to dapa π-backbonding.

3.1. The X-ray structure of $BrMn(CO)_2(N,N,N\text{-dapa})$

Single crystals of $(CO)_5ReMn(CO)_2(N,N,N\text{-dapa})$ could not be obtained. Thus the tridentate coordination of the dapa ligand was confirmed instead for the complex $BrMn(CO)_2(N,N,N\text{-dapa})$. Fig. 3 presents the ORTEP drawing of this complex.

The dapa ligand is present in an in-plane coordination mode, as in all other reported crystal structures of complexes in which the dapa ligand is tridentately coordinated to a metal centre [15]. The central Mn atom possesses a distorted octahedral geometry, as illustrated by the angles of 77.8° for N_1–Mn–N_2 and 77.9° for N_1–Mn–N_3, and the resulting angle of 155.7° for N_2–Mn–N_3. As a consequence of these small angles, the Mn–N_1 (1.95 Å), Mn–N_2 (2.00 Å) and Mn–N_3 (2.00 Å) bond lengths are somewhat shorter than those in the related complexes *fac*-$ClMn(CO)_3$(Ph, Me-DAB) [16] (DAB = 1,4-diaza-1,3-butadiene), *fac*-$BrMn(CO)_3$-(cHex-DAB) [17] and *fac*-$IMn(CO)_3$(bpy) [18]. Both the Br^- and the axial CO ligand are bent towards the equatorial CO ligand, as evidenced by the Br–Mn–C_{22} and C_{23}–Mn–C_{22} angles of 85.6° and 86.5°, respectively. Moreover, the Mn-dapa metallacycle is slightly bent out of plane towards the Br^-, as illustrated by the bond angles Br–Mn–N_1 (85.5°), Br–Mn–N_2 (89.0°) and Br–Mn–N_3 (89.3°). As a result, the C_{23}–Mn–N_1 angle (102.3°) is considerably enlarged.

3.2. Photochemistry

The photochemical reactions of the metal–metal bonded complexes under study were performed in different solvents at various temperatures, both in the absence and presence of PR_3 and the radical scavenger CBr_4. The products obtained were mainly identified by comparing their IR spectral data with those in the literature data, or, in the case of radicals, by simulating the ESR spectra. Most IR data for products and reference compounds are presented only in Table 5; this is especially the case for the products of the $\cdot M(CO)_5$ radicals, which have been identified previously following photolysis of $M_2(CO)_{10}$ in various media with a great variety of reactants.

3.2.1. Photochemistry of fac-$(CO)_5MRe(CO)_3$(N,N-dapa) (M = Mn, Re)

The ^{1}H-NMR spectra of the complexes *fac*-$(CO)_5MRe(CO)_3$(N,N-dapa) (M = Mn, Re) showed two methyl proton singlets at 2.77 and 2.52 ppm for M = Mn and at 2.76 and 2.52 ppm for M = Re. This points to a bidentate coordination of dapa to Re. In agreement with previous results [1i,19], the lowest-energy absorption band of these complexes belongs to MLCT transitions to the lowest π^* orbital of the dapa ligand.

3.2.2. Photolysis at room temperature

Irradiation of the complexes in THF at room temperature in the presence of a 100-fold excess of the radical scavenger CBr_4 gave $BrM(CO)_5$ [20] and *fac*-$BrRe(CO)_3$(N,N-dapa) (*vide supra*) as the only products. The same products were formed thermally, although at a much lower rate. This means that in solution the complexes are already partly dissociated into the radicals $\cdot M(CO)_5$ and $Re^+(CO)_3$(N,N-$dapa^-$). When *fac*-$(CO)_5ReRe(CO)_3$(N,N-dapa) was irradiated in either toluene or THF, a colourless complex was formed having a broad IR CO band at 2011 cm^{-1}. In order to allow identification of this product, the reaction was performed on a preparative scale for a solution of 50 mg *fac*-$(CO)_5ReRe(CO)_3$(N,N-dapa) in 100 ml THF. After completion of the reaction, the solution was concentrated to 3 ml and then transferred to a column packed with Silica 60. After elution with hexane, the colourless product was isolated, and identified as $HRe(CO)_5$ by comparing its CO-stretching frequencies with published data [21]. The formation of this complex shows that the $Re(CO)_5$ radicals, formed by homolysis of the Re–Re bond, do not easily dimerize, but abstract a hydrogen atom from a solvent molecule.

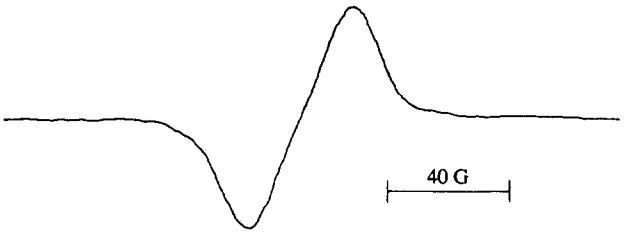

Fig. 4. ESR spectrum of $Re^+(CO)_3(N,N\text{-dapa}^-)$(toluene) in toluene at room temperature.

This latter conclusion was confirmed by dissolving the complex *fac*-$(CO)_5ReRe(CO)_3(N,N\text{-dapa})$ in hexafluorobenzene; the main photoproduct was $FRe(CO)_5$, and again no $Re_2(CO)_{10}$ was found. Only when the concentration of the complex was > 0.2 M were traces of $Re_2(CO)_{10}$ detected. In contrast, irradiation of *fac*-$(CO)_5MnRe(CO)_3(N,N\text{-dapa})$ in THF or toluene gave rise to $Mn_2(CO)_{10}$ [22] as the main product, and no $HMn(CO)_5$ was detected.

The photoreactions of the two complexes were also monitored by ESR spectroscopy. Irradiation of a solution of *fac*-$(CO)_5ReRe(CO)_3(N,N\text{-dapa})$ in toluene resulted in the development of a broad ESR signal (Fig. 4), which upon prolonged irradiation was transformed into the well-resolved signal of Fig. 5A. The same sequence of ESR signals was observed for the corresponding *fac*-$(CO)_5MnRe(CO)_3(N,N\text{-dapa})$ complex. Computer simulation (Fig. 5B, Table 6) revealed that

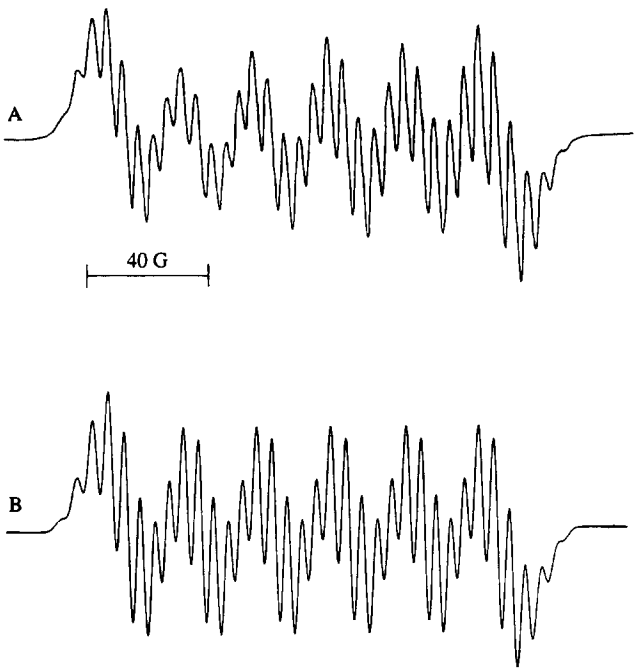

Fig. 5. Experimental (A) and computer-simulated (B) ESR spectrum of $Re^+(CO)_3(N,N,N\text{-dapa}^-)$ in cyclohexane at 323 K.

TABLE 6. Coupling constants (Gauss) of the $Re^+(CO)_3(N,N,N\text{-dapa}^-)$ and $Re^+(CO)_3(N,N\text{-dapa}^-)(PR_3)$ (R = Ph, ^{n}Bu) radical complexes

Radical	a_{Re}	a_N	a_H	a_P
$Re^+(CO)_3(N,N,N\text{-dapa}^-)$ [a]	23.30	4.68	4.68 [b]	
$Re^+(CO)_3(^i\text{Pr-PyCa}^-)$ [c]	28.14	5.54	4.65	
$Re^+(CO)_3(N,N\text{-dapa}^-)(PPh_3)$ [d]	26.78	4.46	4.46 [b]	31.57
$Re^+(CO)_3(N,N\text{-dapa}^-)(P(^n\text{Bu})_3)$ [e]	27.30	4.45	4.45 [b]	30.10

[a] In cyclohexane at 323 K; Linewidth of simulation: 4.10 G. [b] Meta hydrogens of pyridine ring. [c] In toluene at 243 K, from ref. 23. [d] In toluene at 293 K; Linewidth of simulation: 4.20 G. [e] In toluene at 293 K; Linewidth of simulation: 4.25 G.

the ESR signal shown in Fig. 5A is composed of hyperfine couplings with one Re nucleus, three N nuclei and two H nuclei of the pyridine ring of dapa. This spectrum is therefore assigned to the hexa-coordinated radical complex $Re^+(CO)_3(N,N,N\text{-dapa}^-)$. The observation of the same hyperfine coupling for all three N-nuclei is not unexpected, since a similar result was obtained previously for the two N-nuclei of the closely related radical complex $Re^+(CO)_3(^i\text{Pr-PyCa}^-)$ (Table 6) [23]. The formation of the radical $Re^+(CO)_3(N,N,N\text{-dapa}^-)$ has also been studied spectroelectrochemically by one-electron reduction of $XRe(CO)_3(N,N\text{-dapa})$ ($X = Br^-$, Otf^-) inside an IR OTTLE cell [24]. Upon reduction a fast dissociation of X from the reduced parent complex took place. In contrast to the isostructural radical complex $Re^+(CO)_3(^i\text{Pr-PyCa}^-)$, the $Re^+(CO)_3(N,N\text{-dapa}^-)$ radicals formed after release of X did not dimerize. Instead, a mononuclear species was formed giving CO-stretching frequencies at 2000s, 1887s and 1860s cm^{-1} for both $X = Br^-$ and Otf^-. Formation of the solvated radical $Re^+(CO)_3(N,N\text{-dapa}^-)(S)$ (S = THF) could be excluded in this case since such an adduct was not formed upon reduction of the corresponding complexes $XRe(CO)_3(^i\text{Pr-PyCa})$. The above CO bands were therefore assigned to $Re^+(CO)_3(N,N,N\text{-dapa}^-)$ [24]. In agreement with this assignment, the radical was converted into $[Re(CO)_3(N,N,N\text{-dapa})]^+$ upon reoxidation.

The same sequence of ESR signals was observed for the complexes dissolved in toluene, THF or cyclohexane. In cyclohexane the broad ESR signal (Fig. 4) was, however, more readily transformed than in toluene, into the well-resolved signal of $Re^+(CO)_3(N,N,N\text{-dapa}^-)$ (Fig. 5A), and this transformation was much slower in THF. This implies that the stability of the paramagnetic species responsible for the broad ESR signal increases with increasing coordinating ability of the solvent. As shown above this species, which is assigned as $Re^+(CO)_3(N,N\text{-dapa}^-)(S)$ (S = solvent molecule), was not observed spectroelectrochemically.

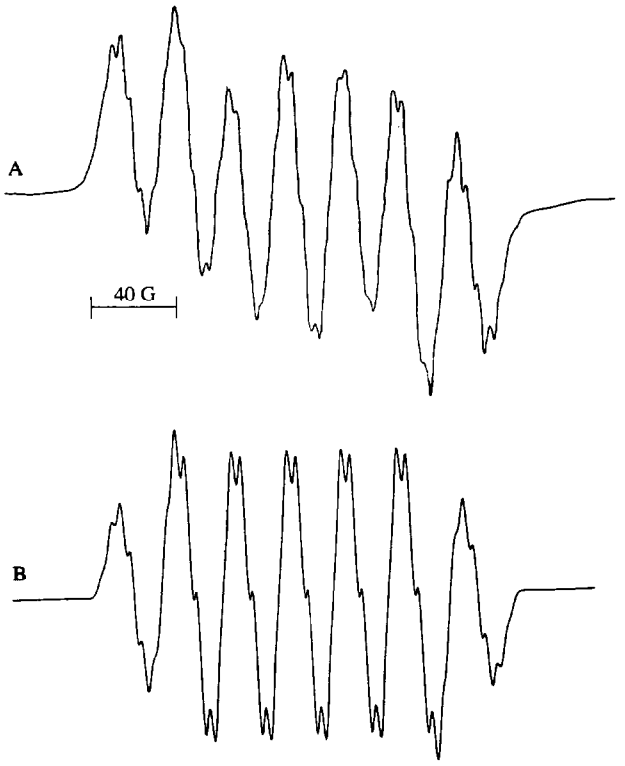

Fig. 6. Experimental (A) and computer-simulated (B) ESR spectrum of $Re^+(CO)_3(N,N\text{-dapa}^-)(PPh_3)$ in toluene at room temperature.

When, after complete formation of the radical $Re^+(CO)_3(N,N,N\text{-dapa}^-)$, an excess of PR_3 (R = Ph, ^{n}Bu) was added to the solution, the ESR signal of Fig. 5A was transformed into that shown in Fig. 6A. Apparently, one of the imine-nitrogen atoms had been replaced by PR_3, giving the radical $Re^+(CO)_3(N,N\text{-dapa}^-)(PR_3)$, which, on the basis of previous observations probably has a facial geometry [23]. This conclusion was supported by computer simulation (Fig. 6B, Table 6). A large hyperfine coupling with the P nucleus dominated the ESR spectrum. In addition, hyperfine couplings with one Re, two N and two H nuclei were observed. The conversion of $Re^+(CO)_3(N,N,N\text{-dapa}^-)$ into $Re^+(CO)_3(N,N\text{-dapa}^-)(PR_3)$ shows that PR_3 coordinates more strongly to the Re centre than does the third nitrogen atom of the dapa ligand.

Although the ESR spectra clearly show the formation of the radical $Re^+(CO)_3(N,N,N\text{-dapa}^-)$, this observation could not be confirmed by the IR spectra. Apart from the intense, broad CO band of $HRe(CO)_5$ or the corresponding bands of $Mn_2(CO)_{10}$, only weak additional IR bands were observed for both complexes at 2020, 1922, 1901, 1887, 1870 cm^{-1} in THF, and 2022, 1929, 1897 cm^{-1} in toluene. Neither of these bands belong to $Re^+(CO)_3(N,N,N\text{-dapa}^-)$ (*vide supra*). They are tentatively assigned to the cation $Re(CO)_3(N,N,N\text{-dapa})^+$, which has also been identified spectroelectrochemically (ν(CO) in THF: 2022s, 1925s, 1900s cm^{-1}) [24]. The weak bands at 1887 and 1870 cm^{-1}, observed in THF, were not assigned.

The above results show that, according to the ESR spectra and by comparison with the spectroelectrochemical data, the $Re^+(CO)_3(N,N,N\text{-dapa}^-)$ radical is formed upon irradiation of these metal-metal bonded complexes, but that the concentration of this radical is too low to be detected by IR spectroscopy.

Irradiation of *fac*-$(CO)_5MRe(CO)_3(N,N\text{-dapa})$ in the presence of a 100-fold excess of PPh_3 or $P(^nBu)_3$ gave a more straightforward result. For M = Re and in the presence of PPh_3 two products were formed in THF, and were identified as *cis*-$HRe(CO)_4(PPh_3)$ [25] and $Re^+(CO)_3(N,N\text{-dapa}^-)(PPh_3)$ from their IR spectra. The latter radical could be identified in this way by comparison of its IR data with those obtained recently for this product during a spectroelectrochemical study of the parent *fac*-$BrRe(CO)_3(N,N\text{-dapa})$ complex in the presence of PPh_3 [24]. When the reaction was performed in THF in the presence of a 100-fold excess of $P(^nBu)_3$, three products were formed. These were identified as *cis*-$HRe(CO)_4(P(^nBu)_3)$, *mer,trans*-$HRe(CO)_3(P(^nBu)_3)_2$ and the radical complex $Re^+(CO)_3(N,N\text{-dapa}^-)(P(^nBu)_3)$ by comparing their IR spectra with published data for *cis*-$HRe(CO)_4(PEt_3)$ [26], *mer,trans*-$HRe(CO)_3(PEt_3)_2$ [26] and $Re^+(CO)_3(N,N\text{-dapa}^-)(PPh_3)$ [24] (Table 5).

The corresponding Mn complex *fac*-$(CO)_5MnRe(CO)_3(N,N\text{-dapa})$ gave a variety of products upon irradiation in toluene in the presence of PPh_3. The $\cdot Mn(CO)_5$ radicals reacted to give $Mn_2(CO)_{10}$, $Mn(CO_5^-$ [27] and $Mn_2(CO)_9(PPh_3)$ [28], as evidenced by their IR spectra. The $Re^+(CO)_3(N,N\text{-dapa}^-)$ radicals, formed by the homolysis reaction, produced $Re^+(CO)_3(N,N\text{-dapa}^-)(PPh_3)$ and the cation $Re(CO)_3(N,N\text{-dapa})(PPh_3)^+$ [24]. The formation of this cation and $Mn(CO)_5^-$ shows that an electron transfer reaction had taken place between the $Re^+(CO)_3(N,N\text{-dapa}^-)(PPh_3)$ radical complex and the $\cdot Mn(CO)_5$ radical still present in the solvent cage. This conclusion was confirmed by the observation that a larger amount of the cation was formed in the more viscous THF solution at 203 K (*vide infra*).

Thus, according to both the IR and ESR spectra, the two metal–metal bonded complexes produce the radical species $Re^+(CO)_3(N,N\text{-dapa}^-)(PPh_3)$ as the main product of the $Re(CO)_3(N,N\text{-dapa})$ fragment. Apparently, these radicals are much more stable than the $Re^+(CO)_3(N,N,N\text{-dapa}^-)$ radical, which could only be detected by ESR spectroscopy and not by the less sensitive IR technique.

3.2.3. Photolysis at low temperature

Irradiation of *fac*-$(CO)_5MnRe(CO)_3$(N,N-dapa) in toluene at 203 K gave $Mn_2(CO)_{10}$ as the main product and $Mn(CO)_5^-$ in low concentration. Another product was formed in a comparably low concentration and gave IR CO bands at 2024s, 1918s and 1901s cm^{-1}. These frequencies closely resemble those for $Re(CO)_3$-(N,N,N-dapa)$^+$ (ν(CO) in THF: 2022s, 1925s and 1900s cm^{-1}), which were determined spectroelectrochemically in THF [24], and so are therefore assigned to this cation.

Irradiation of *fac*-$(CO)_5ReRe(CO)_3$(N,N-dapa) in THF at 203 K gave a much smaller amount of $HRe(CO)_5$ than did the photoreaction at room temperature. Instead, both $Re_2(CO)_{10}$ [22] and $Re(CO)_5^-$ [27] were formed as the main products from the $\cdot Re(CO)_5$ radicals. The other product of the homolysis reaction, the 16-electron $Re^+(CO)_3$(N,N-dapa$^-$) radical complex, gave rise to three products. One of these gave CO bands at 2021s, 1918s and 1898s cm^{-1} and was therefore identified as $Re(CO)_3$(N,N,N-dapa)$^+$, just as for the above reaction of *fac*-$(CO)_5MnRe(CO)_3$(N,N-dapa). The second product was identified as $Re(CO)_3$(N,N-dapa)(THF)$^+$ because of the close similarity of its IR CO bands with those of $Re(CO)_3$(bpy)(2-MeTHF)$^+$ [29]. The third product was judged to be the radical complex $Re^+(CO)_3$ (N,N-dapa$^-$)(THF) because its CO-stretching frequencies (2008s, 1897s and 1887s cm^{-1}) are very similar to those of $Re^+(CO)_3$-(N,N-dapa$^-$)(CH_3CN) [24] and $Re^+(CO)_3$(dpp$^-$)(THF) (dpp = 2,3-bis(2-pyridyl)pyrazine) [24] (see Table 5).

In order to prove that the ions formed in the above reaction resulted from homolysis of the metal–metal bond followed by electron transfer between the radicals, and not from a heterolytic splitting of the metal–metal bond, the complexes were also irradiated in THF at 203 K in the presence of CBr_4. The complexes $BrM(CO)_5$ and *fac*-$BrRe(CO)_3$(N,N-dapa) were then formed as the only products. This implies that metal–metal bond homolysis is indeed the primary photoprocess in the formation of ions such as $Re(CO)_3$(N,N,N-dapa)$^+$ and $M(CO)_5^-$. A similar mechanism of homolysis followed by electron transfer was proposed previously for the closely related complex *fac*-$(CO)_5MnRe(CO)_3$(bpy) [1h].

The main difference between the reactions at low temperature and room temperature is the formation of ions in the former case. At low temperature, diffusion of the radicals from the solvent cage will be hampered by the increased viscosity of the solvent. As a result, these radicals will stay together and more easily undergo electron transfer reactions. At the same time, the ions formed will be more stabilized by the solvent molecules, because of their increased coordinating ability at this temperature. A further difference is that the $\cdot Re(CO)_5$ radicals, not involved in the electron transfer reaction, produced $Re_2(CO)_{10}$ at lower temperatures and $HRe(CO)_5$ at room temperature. This temperature effect was confirmed by performing the photoreaction of *fac*-$(CO)_5ReRe(CO)_3$(N,N-dapa) in 2-MeTHF at 293, 243, 193 and 143 K. At 293 and 243 K the products were the same as those in THF at room temperature. At 193 and 143 K again $Re(CO)_5^-$, $Re(CO)_3$(N,N-dapa)(2-MeTHF)$^+$, $Re_2(CO)_{10}$ and $Re^+(CO)_3$(N,N-dapa$^-$)(2-MeTHF) were formed.

Photolysis of *fac*-$(CO)_5ReRe(CO)_3$(N,N-dapa) in THF at 203 K in the presence of a 100-fold excess of PR_3 (R = Ph, ^{n}Bu) gave a mixture of products. For the reaction with $P(^nBu)_3$ the products *mer,trans*-$HRe(CO)_3(P(^nBu)_3)_2$ and $Re^+(CO)_3$(N,N-dapa$^-$)($P(^nBu)_3$) were the same as those formed at room temperature (*vide supra*). In addition, $Re_2(CO)_9$-($P(^nBu)_3$) was formed, and was identified by the close resemblance of its CO-stretching frequencies with those of $Re_2(CO)_9(PMe_3)$ [30]. Finally, the two ionic compounds $Re(CO)_5^-$ and $Re(CO)_3$(N,N-dapa)($P(^nBu)_3$)$^+$ were formed. The latter complex ion was identified by the close correspondence of its CO bands with those from $Re(CO)_3$(N,N-dapa)(PPh_3)$^+$ [24] (Table 5 and *vide supra*). Reaction of the complex in THF at 203 K in the presence of an excess of PPh_3 gave *cis*-$HRe(CO)_4(PPh_3)$ and $Re^+(CO)_3$(N,N-dapa$^-$)(PPh_3), which were also observed when the reaction was performed at room temperature. In addition, $Re_2(CO)_9$-(PPh_3) [30] was formed as a third product.

Photolysis of the complex *fac*-$(CO)_5MnRe(CO)_3$-(N,N-dapa) in toluene at 203 K in the presence of an excess of PPh_3 gave the same products as those formed at room temperature.

The above results show that the two complexes under study undergo homolysis of the metal–metal

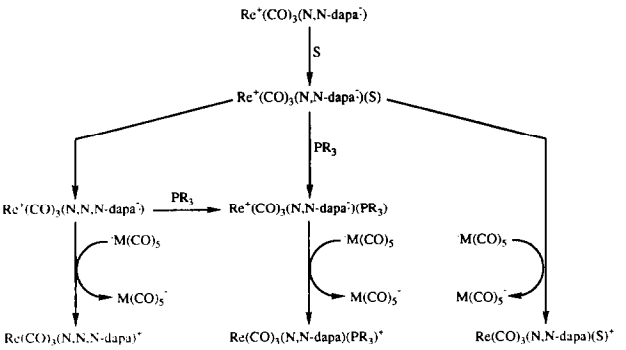

Scheme 1.

bond. At low temperatures this reaction is partly followed by electron transfer between the radicals. Similar results have been obtained for the related complexes *fac*-$(CO)_5MRe(CO)_3$(bpy) [1h]. The crucial point is that the third nitrogen donor atom of the dapa ligand only weakly stabilizes the 16-electron $Re^+(CO)_3$(N,N-dapa$^-$) radical to give the coordinatively saturated complex $Re^+(CO)_3$(N,N,N-dapa$^-$), since the latter radical could only be detected with ESR spectroscopy and the third nitrogen was also very readily replaced by PR_3 or, at low temperatures, by a coordinating solvent such as THF. The various reactions of the $Re^+(CO)_3$(N,N-dapa$^-$) radical are shown in Scheme 1.

3.2.4. Photochemistry of $(CO)_5ReMn(CO)_2$(N,N,N-dapa)

Irradiation of this complex in THF or toluene at room temperature in the presence of a 100-fold excess of CBr_4 gave $BrRe(CO)_5$ as the main product. Owing to its photolability, only traces of $BrMn(CO)_2$(N,N,N-dapa) were observed, but formation was evident in the thermal reaction, with exclusion of light, of the metal-metal complex with CBr_4. Under these conditions $BrRe(CO)_5$ and $BrMn(CO)_2$(N,N,N-dapa) were formed in equal amounts.

Irradiation of the complex in various solvents (THF, hexane, toluene *etc.*) in the absence of any other reactant gave $HRe(CO)_5$ as the main product, together with a very small amount of $Re(CO)_5^-$. The formation of the latter product points to occurrence of a disproportionation reaction, as a result of the electron transfer between the $Mn^+(CO)_2$(N,N,N-dapa$^-$) and $\cdot Re(CO)_5$ radicals formed by homolysis of the metal–metal bond. No products from the $Mn(CO)_2$(N,N,N-dapa) part of the parent complex could be detected. Apparently, both the radical $Mn^+(CO)_2$(N,N,N-dapa$^-$) and the cation $Mn(CO)_2$(N,N,N-dapa)$^+$ readily decompose. The radical could also not be detected by ESR spectroscopy, even after addition of the spin-trapping agent ^{t}Bu-NO to the solution. This illustrates the low stability of this radical.

Irradiation of the complex at room temperature in the presence of a 100-fold excess of PR_3 (R = Ph, ^{n}Bu) gave rise to the formation of a mixture of $HRe(CO)_5$ and the substitution products $HRe(CO)_{5-x}(PR_3)_x$ (x = 1, 2), just as for *fac*-$(CO)_5ReRe(CO)_3$(N,N-dapa) (*vide supra*).

Photolysis of the complex in THF or toluene at 203 K or in 2-MeTHF at 133 K gave $Re(CO)_5^-$, $HRe(CO)_5$ and a third product which has not yet been identified. As in the case of the *fac*-$(CO)_5MRe(CO)_3$(N,N-dapa) complexes, $Re(CO)_5^-$ was formed in a much higher concentration than at room temperature, and only a small amount of $HRe(CO)_5$ was formed.

3.2.5. Photochemistry of fac-$(CO)_5MM'(CO)_3$(N,N-map) (M, M' = Mn, M, M' = Re; M = Re, M' = Mn)

The photochemistry of these complexes was studied at various temperatures in THF and toluene. The complexes *fac*-$(CO)_5MnMn(CO)_3$(N,N-map) behaved like the related compounds *fac*-$(CO)_5MnMn(CO)_3$(α-diimine), which were studied recently [1e]. Irradiation in the presence of excess CBr_4 gave $BrMn(CO)_5$ and *fac*-$BrMn(CO)_3$(N,N-map), while $Mn_2(CO)_{10}$ and $Mn_2(CO)_6$(N,N-map)$_2$ were produced upon excitation in the absence of any reactant. The dimer $Mn_2(CO)_6$(N,N-map)$_2$ showed a strong MLCT band at very low energy (λ_{max} = 820 nm in THF), which has also been observed for the related $Mn_2(CO)_6$(α-diimine)$_2$ complexes [1d,e]. The formation of this dimer indicates that no stable $Mn^+(CO)_3$(N,N,N-map$^-$) radicals were formed from the primary photoproduct $Mn^+(CO)_3$(N,N-map$^-$). In agreement with this, no ESR signal was observed during the photolysis reaction.

In contrast, at low temperatures the complexes *fac*-$(CO)_5MnMn(CO)_3$(α-diimine) were shown to undergo release of CO from the $Mn(CO)_3$(α-diimine) fragment to form the CO-bridged species $(CO)_4Mn(\mu$-CO)$Mn(CO)_2$(α-diimine) [1e]. In the case of the complex *fac*-$(CO)_5MnMn(CO)_3$(N,N-map) a similar product $(CO)_4Mn(\mu$-CO)$Mn(CO)_2$(N,N-map) was formed upon irradiation in 2-MeTHF at 133 K. This was evident from the close correspondence between its CO-stretching frequencies and those of $(CO)_4Mn(\mu$-CO)$Mn(CO)_2$(^{i}Pr-PyCa) [1e]. For both products the lowest-frequency CO band, belonging to the bridging CO ligand, was observed at 1821 cm^{-1}. It is noteworthy that after release of CO from the $Mn(CO)_3$(N,N-map) fragment the vacant site is not occupied by the third nitrogen donor atom of map, but by a CO ligand of the $Mn(CO)_5$ fragment. Raising the temperature to 183 K caused a back-reaction with CO still present in the solution to regenerate the parent complex. In order to find out whether the bridging CO could be replaced by the nitrogen donor side-arm of map, the solution containing the product of CO-loss was raised in temperature after removal of CO from the reaction mixture. This was accomplished by performing the photoreaction in a Low Temperature Free Access InfraRed (LT FAIR) cell [8]. This cell is in fact a combination of a reaction vessel and a closely connected IR measurement cell. Bubbling of cooled N_2 through the irradiated solution in the reaction vessel at 133 K, removed free CO from the reaction mixture. Raising the temperature to 183 K then caused a shift of the 1821 cm^{-1} band, while the other CO bands hardly

changed in frequency. A similar behaviour of the CO-stretching frequencies was observed earlier when the CO-loss product $(CO)_4Mn(\mu\text{-}CO)Mn(CO)_2(bpy)$ was converted into $(CO)_5MnMn(CO)_2(bpy)$(pyridine) by raising the temperature of its solution in 2-MeTHF from 133 to 203 K in the presence of pyridine [1e]. We therefore suggest that raising the temperature of a solution of $(CO)_4Mn(\mu\text{-}CO)Mn(CO)_2$(N,N-map) in the absence of CO gives rise to the formation of $(CO)_5MnMn(CO)_2$(N,N,N-map). Support for this conclusion was obtained by a further increase in temperature; the frequencies of the product of CO loss were still observed at 268 K, whereas all the $(CO)_4Mn(\mu\text{-}CO)Mn(CO)_2(\alpha\text{-diimine})$ complexes studied are only stable below 223 K [1e].

The above results show that, in contrast to the reaction at room temperature, no homolysis products are formed at these low temperatures. This was also evident from the photoreaction of the complex in 2-MeTHF at 133 K in the presence of CBr_4, which only produced a very small amount of $BrMn(CO)_5$ and *fac*-$BrMn(CO)_3$(N,N-map). It is not yet clear if this effect is due to the high viscosity of the solvent at low temperatures, which causes a fast back-reaction of the radicals within the solvent case, or to lack of thermal energy needed for the population of the reactive state responsible for the homolysis reaction.

When the photoreaction was performed at an intermediate temperature (T = 203 K) in THF or toluene, products of both the homolysis and the CO-loss reaction were observed. Again, the CO-loss product was $(CO)_4Mn(\mu\text{-}CO)Mn(CO)_2$(N,N-map). The homolysis reaction produced $Mn_2(CO)_{10}$, which indicates that the $\cdot Mn(CO)_5$ radicals can diffuse from the solvent cage at this temperature. In contrast to their behaviour at room temperature, the $Mn^+(CO)_3$(N,N-map$^-$) radicals did not simply dimerize to give $Mn_2(CO)_6$(N,N-map)$_2$, but instead formed a complex having CO-stretching frequencies at 1971s, 1985s, br cm^{-1} in THF and 1972s, 1894s, br cm^{-1} in toluene. These values are almost identical to those for the binuclear complex $Mn_2(CO)_4(\sigma,\sigma,\eta^2\text{-}^i\text{Pr-DAB})_2$, formed as a stable intermediate upon irradiation of *fac*-$(CO)_5MnMn(CO)_3(^i\text{Pr-DAB})$ at low temperatures [1e]. In this product both ^{i}Pr-DAB ligands are σ,σ-coordinated to one Mn atom and η^2-bonded to the other via an imine bond. The product of the corresponding map complex is therefore suggested to be $Mn_2(CO)_4(\sigma,\sigma,\eta^2\text{-N,N-map})_2$. A further increase in temperature caused conversion of this product into $Mn_2(CO)_6$(N,N-map)$_2$, which is one of the two photoproducts formed at room temperature (*vide supra*).

In agreement with recent results for several complexes of the type *fac*-$(CO)_5ReMn(CO)_3(\alpha\text{-diimine})$ [1g], irradiation of *fac*-$(CO)_5ReMn(CO)_3$(N,N-map) also gave rise to release of CO at low temperature. Again, a CO-bridged complex was formed having very similar CO-stretching frequencies as those for the corresponding complex $(CO)_4Re(\mu\text{-}CO)Mn(CO)_2(bpy)$ [1g]. The bridging CO ligands of the map and bpy complexes had their stretching frequencies at 1808 and 1805 cm^{-1}, respectively. When this low temperature reaction was performed instead in 2-MeTHF in a LT FAIR cell [8] and CO was removed from the solution after photolysis, the CO-bridged product of the map complex was transformed into a different compound upon raising of the temperature. This complex had its lowest-frequency band shifted from 1808 to 1824 cm^{-1}, while all other CO bands hardly changed in frequency. As for *fac*-$(CO)_5MnMn(CO)_3$(N,N-map), this product is suggested to be $(CO)_5ReMn(CO)_2$(N,N,N-map), formed from the CO-bridged complex by replacement of the CO-bridge by the nitrogen donor side-arm of the map ligand. However, in contrast to the corresponding $(CO)_5MnMn(CO)_2$(N,N,N-map) complex, $(CO)_5ReMn(CO)_2$(N,N,N-map) was formed as a stable photoproduct even at room temperature, along with $HRe(CO)_5$ and $Mn_2(CO)_6$(N,N-map)$_2$.

The complex *fac*-$(CO)_5ReRe(CO)_3$(N,N-map) only underwent homolysis of the metal–metal bond. Photolysis in THF at room temperature or at 203 K in the presence of CCl_4 gave $ClRe(CO)_5$ and *fac*-$ClRe(CO)_3$(N,N-map) as the only products. When this reaction was performed in THF or toluene at 203 K or in 2-MeTHF at 143 K in the absence of any reactant, a product with seven CO bands at 2075m, 2021vs, 1972s, 1966s, 1928s, 1915s and 1902s cm^{-1} was formed (Fig. 7), together with a very small amount of $HRe(CO)_5$. No free CO was then observed, which means that the observed product had been formed by a homolysis reaction. The absorption spectrum showed the disappearance of the visible band of the starting complex, while a shoulder showed up at 330 nm as the only product band between 300 and 900 nm. Apart from the small amount of $HRe(CO)_5$, there was no indication of the formation of any other product from the $Re(CO)_5$ radicals such as $Re_2(CO)_{10}$ or $Re(CO)_5^-$. This behaviour, which contrasts with that of the corresponding *fac*-$(CO)_5ReRe(CO)_3$(N,N-dapa) complex, shows that the $Re(CO)_5$ radicals are involved in the formation of the product giving the seven CO-stretching frequencies. Moreover, these frequencies do not deviate much from those for the parent complex and for the corresponding compound *fac*-$(CO)_5ReRe(CO)_3$(N,N-dapa). Apparently, we are dealing here with a binuclear Re–Re bonded complex still containing the $Re(CO)_5$ and $Re(CO)_3$(N,N-map) groups. The disappearance of the visible absorption band shows that the map ligand is no

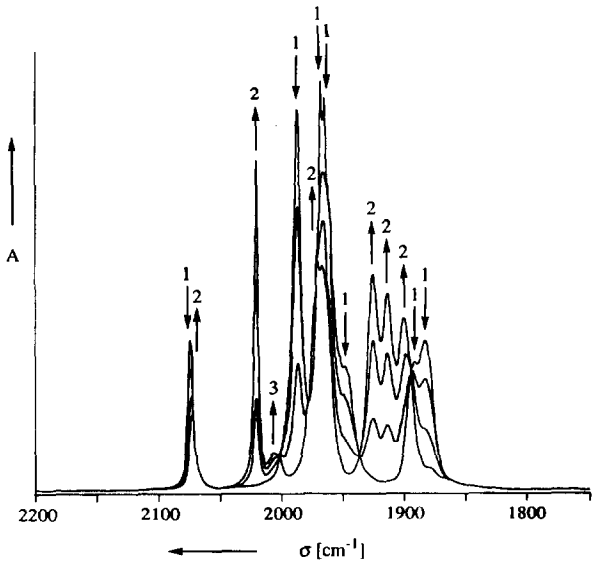

Fig. 7. IR (CO-stretching region) spectral changes during the photochemical reaction of *fac*-$(CO)_5ReRe(CO)_3(N_1,N_2\text{-map})$ in THF at 203 K; 1 = *fac*-$(CO)_5ReRe(CO)_3(N_1,N_2\text{-map})$, 2 = $(CO)_5ReRe(CO)_3(N_2,N_3\text{-map})$, 3 = $HRe(CO)_5$.

longer coordinated to the metal via its conjugated N_1–C–C–N_2 (pyridine-imine) skeleton, but instead probably via the two nitrogen atoms N_2 and N_3, and so we judge the product to be $(CO)_5ReRe(CO)_3(N_2,N_3\text{-map})$. Up to now, we have not been able to obtain firm proof for the proposed structure owing to the thermal instability of the product at higher temperatures.

The $Re^+(CO)_3(N,N\text{-map}^-)$ radicals, formed by the homolysis of the *fac*-$(CO)_5ReRe(CO)_3(N,N\text{-map})$ complex, gave rise to a broad ESR signal, which disappeared upon prolonged irradiation. As for the corresponding dapa complex, this signal is assigned to the solvent-stabilized $Re^+(CO)_3(N,N\text{-map}^-)(S)$ radical. Apparently, the unfavourable bounding in the radical through the charged pyridine group is changed into coordination via the neutral pyridine. Back-reaction with a $\cdot Re(CO)_5$ radical then produces the complex $(CO)_5ReRe(CO)_3(N_2,N_3\text{-map})$, which is, however, much less stable than the parent complex. In contrast to the results for the dapa complex, the ESR signal did not change into that of the coordinatively saturated radical $Re^+(CO)_3(N,N,N\text{-map}^-)$, probably because of the reported change of the structure of the radical to give $(CO)_5ReRe(CO)_3(N_2,N_3\text{-map})$.

Upon irradiation of *fac*-$(CO)_5ReRe(CO)_3(N,N\text{-map})$ at room temperature in the presence of an excess of PR_3 (R = Ph, ^{n}Bu), the products were similar to those formed from the corresponding dapa complex. However, when the map complex was irradiated in THF at 203 K in the presence of PPh_3, the same products were formed as in the absence of this reactant, whereas for the dapa complex a reaction of the PPh_3 ligand with the photochemically formed radicals was observed (*vide supra*). This difference in behaviour may be connected with the structural change of the $Re^+(CO)_3(N,N\text{-map}^-)$ radical, mentioned above.

4. Summary and conclusions

As stated in the Introduction, complexes of the type *fac*-$(CO)_5MM'(CO)_3(\alpha\text{-diimine})$ (M, M' = Mn, Re) undergo homolysis of the M–M' bond and/or release of CO, according to reactions 4 and 5, respectively, upon irradiation into their visible absorption

$$fac\text{-}(CO)_5MM'(CO)_3(\alpha\text{-diimine}) \xrightarrow{h\nu} \cdot M(CO)_5 + M'^+(CO)_3(\alpha\text{-diimine}^-) \quad (4)$$

$$fac\text{-}(CO)_5MM'(CO)_3(\alpha\text{-diimine}) \xrightarrow{h\nu} (CO)_5MM'(CO)_2(\alpha\text{-diimine}) + CO \quad (5)$$

band. The 16-electron $M'^+(CO)_3(\alpha\text{-diimine}^-)$ radicals can initiate electron transfer chain (ETC) reactions provided that their dimerization is prevented by adduct formation with a Lewis base such as PR_3.

The aim of this study was to find a way in which the use of the stabilizing PR_3 ligand could be avoided. As a first approach, complexes, in which the α-diimine is a tridentate ligand coordinated as a chelate in the $M'(CO)_3(\alpha\text{-diimine})$ fragment were prepared and their photochemical behaviour studied. It was expected that the third nitrogen donor atom would stabilize the 16-electron $M'^+(CO)_3(N,N\text{-}\alpha\text{-diimine}^-)$ radical to give the coordinatively saturated 18-electron $M'^+(CO)_3(N,N,N\text{-}\alpha\text{-diimine}^-)$ complex by intramolecular adduct formation. For this purpose, the two α-diimine ligands dapa and map (Fig. 1) were selected. In the case of dapa, coordination as a tridentate ligand was indeed established by ESR spectroscopy for the radical $Re^+(CO)_3(N,N,N\text{-dapa}^-)$, which had been formed by irradiation of *fac*-$(CO)_5MRe(CO)_3(N,N\text{-dapa})$ (M = Mn, Re) (Scheme 1). The concentration of this radical was, however, very low, and it could therefore not be detected by IR spectroscopy. The weakness of the bond between the metal and the third nitrogen donor atom was also evident upon addition of PR_3 to the solution of the radical, the radical complex $Re^+(CO)_3(N,N\text{-dapa}^-)(PR_3)$ immediately being formed in rather high concentration according to the IR spectrum (Scheme 1).

In the case of the corresponding map complexes there was no evidence for tridentate coordination within the radicals. These results show that adduct

formation by a nitrogen donor ligand is unfavourable in the case of these radicals. This behaviour is in agreement with our previous observation that ETC reactions of these *fac*-$(CO)_5MM'(CO)_3$(α-diimine) complexes do not occur if hard bases such as THF, amines or pyridine are used for adduct formation, unless they are present in very large excess (*e.g.* neat pyridine) [1f]. Coordination of the hard bases is very unfavourable, because of the high electron density generated on the metal by the radical anion. A better choice might be an α-diimine ligand with a phosphorus donor side-arm. In that case, however, the α-diimine ligand should be one for which bidentate coordination preferably takes place via the two nitrogen donor atoms and not via N and P. Thus, the α-diimine should have a rigid α-diimine skeleton, such as that of phenanthroline, which imposes this N,N-coordination. We have not yet succeeded in making such a phenanthroline ligand with a phosphorus donor side-arm. The ability of dapa to impose a tridentate coordination is much stronger for the neutral ligand. This was illustrated by the observation that the *fac*-$(CO)_5MMn(CO)_3$(N,N-dapa) complexes could not be made by reaction 1, reaction 2 taking place instead. In the case of *fac*-$BrMn(CO)_3$(N,N-dapa), tridentate coordination to give $BrMn(CO)_2$(N,N,N-dapa) was very easily achieved, thermally, photochemically as well as electrochemically (reaction 3), and this tridentate coordination was confirmed by an X-ray structure determination for $BrMn(CO)_2$(N,N,N-dapa) (Fig. 3).

Again, tridentate coordination was much less favourable in the case of the map complexes. The complexes *fac*-$(CO)_5MMn(CO)_3$(N,N-map) (M = Mn, Re) were readily obtained as stable complexes and *fac*-$BrMn(CO)_3$(N,N-map) only reacted photochemically to give the thermally unstable $BrMn(CO)_2$-(N,N,N-map) species. For the metal–metal bonded complexes, tridentate coordination of map was observed when *fac*-$(CO)_5MMn(CO)_3$(N,N-map) (M = Mn, Re) was irradiated at low temperatures. The CO-bridged complex $(CO)_4M(\mu\text{-}CO)Mn(CO)_2$(N,N-map) thus formed, according to reaction 6, was converted into $(CO)_5MMn(CO)_2$(N,N,N-map) when the temperature was raised in the absence of CO (reaction 7).

$$fac\text{-}(CO)_5MMn(CO)_3(N,N\text{-map}) \xrightarrow{h\nu} (CO)_4M(\mu\text{-}CO)Mn(CO)_2(N,N\text{-map}) + CO \quad (6)$$

$$(CO)_4M(\mu\text{-}CO)Mn(CO)_2(N,N\text{-map}) \xrightarrow{\Delta} (CO)_5MMn(CO)_2(N,N,N\text{-map}) \quad (7)$$

These differences in the behaviour of dapa and map must be mainly due to the much greater tendency of the third nitrogen donor atom of dapa to lie in close proximity to the metal, which is of course essential for good tridentate coordination.

Acknowledgment

We thank the Netherlands Foundation for Chemical Research (SON) and the Netherlands Organization for the Advancement of Pure Research (NWO) for financial support.

Supplementary material available

Listings of the atomic coordinates the anisotropic thermal parameters for non-hydrogen atoms, and a full list of lengths and angles have been deposited at the Cambridge Crystallographic Data Center.

References

1 (a) D.L. Morse and M.S. Wrighton, *J. Am. Chem. Soc., 98* (1976) 3931; (b) M.W. Kokkes, D.J. Stufkens and A. Oskam, *Inorg. Chem., 24* (1985) 2934; (c) M.W. Kokkes, D.J. Stufkens and A. Oskam, *Inorg. Chem., 24* (1985) 4411; (d) M.W. Kokkes, W.G.J. de Lange, D.J. Stufkens and A. Oskam, *J. Organomet. Chem., 294* (1985) 59; (e) T. van der Graaf, D.J. Stufkens, A. Oskam and K. Goubitz, *Inorg. Chem., 30* (1991) 599; (f) T. van der Graaf, R.M.J. Hofstra, P.G.M. Schilder, M. Rijkhoff and D.J. Stufkens, *Organometallics, 10* (1991) 3668; (g) B.D. Rossenaar, T. van der Graaf, R. van Eldik, C.H. Langford, D.J. Stufkers and A. Vlček, Jr., *Inorg. Chem.*, in press; (h) T. van der Graaf, A. van Rooy, D.J. Stufkens and A. Oskam, *Inorg. Chim. Acta, 187* (1991) 133; (i) D.J. Stufkens, *Coord. Chem. Rev., 104* (1990) 39.

2 A. Lavery and S.M. Nelson, *J. Chem. Soc., Dalton Trans.*, (1984) 615.

3 R.E. Rülke, J.M. Ernsting, A.L. Spek, C.J. Elsevier, P.W.N.M. van Leeuwen and K. Vrieze, *Inorg. Chem.*, in press.

4 J.M. Albon, D.A. Edwards and P.J. Moore, *Inorg. Chim. Acta, 159* (1989) 19.

5 G. Brauer, *Handbuch der Präparativen Anorganischen Chemie*, Ferdinand Enke Verlag, Stuttgart, 1981, p. 1950.

6 (a) D.L. Morse and M.S. Wrighton, *J. Organomet. Chem., 125* (1977) 71; (b) L.H. Staal, G. van Koten and K. Vrieze, *J. Organomet. Chem., 175* (1979) 73.

7 B.P. Sullivan and T.J. Meyer, *J. Chem. Soc., Chem. Commun.*, (1984) 1244.

8 P.G.M. Schilder, H. Luyten, D.J. Stufkens and A. Oskam, *Appl. Spectrosc., 45* (1991) 1344. The FAIR cells are sold by Bio-Rad Analytical Instruments Group.

9 M. Krejcik, M. Danek and F. Hartl, *J. Electroanal. Chem., Interfacial Electrochem., 317* (1991) 179.

10 N. Walker and D. Stewart, *Acta Crystallogr., Sect. A: Found Crystallogr., A39* (1983) 158.

11 (a) D.T. Cromer and J.B. Mann, *Acta Crystallogr., Sect. A: Cryst. Phys. Diffr. Theor. Gen. Crystallogr. A24* (1968) 321; (b) D.T. Cromer and J.B. Mann, *International Tables for X-Ray Crystallography*, Kynoch Press, Birmingham, UK, 1974, Vol. IV, p. 55.

12 S.R. Hall and J.M. Stewart, (eds.), XTAL3.0 *Users Manual*, Universities of Western Australia and Maryland.

13 J.K. Kochi, *J. Organomet. Chem., 300* (1986) 139.

14 D. Miholovà and A.A. Vlcek, *J. Organomet. Chem., 279* (1985) 317.
15 (a) E.C. Alyea, G. Ferguson and R.J. Restivo, *Inorg. Chem., 14* (1975) 2491; (b) R.J. Restivo and G. Ferguson, *J. Chem. Soc., Dalton Trans.,* (1976) 518; (c) A.J. Blake, A.J. Lavery, T.I. Hyde and M. Schröder, *J. Chem. Soc., Dalton Trans.,* (1989) 965; (d) D.A. Edwards, M.F. Mahon, W.R. Martin, K.C. Molloy, P.E. Fanwick and R.A. Walton, *J. Chem. Soc., Dalton Trans.,* (1990) 3161.
16 G. Schmidt, H. Paulus, R. van Eldik and H. Elias, *Inorg. Chem., 28* (1988) 3211.
17 A.J. Graham, B. Akrigg and B. Sheldrick, *Cryst. Struct. Commun., 6* (1977) 571.
18 G.J. Stor, D.J. Stufkens, P. Vernooijs, E.J. Baerends, J. Fraanje and K. Goubitz, to be published.
19 M.W. Kokkes, T.L. Snoeck, D.J. Stufkens, A. Oskam, M. Christophersen and C.H. Stam, *J. Mol. Struct., 131* (1985) 11.
20 J.C. Hileman, D.K. Huggins and H.D. Kaesz, *Inorg. Chem., 1* (1962) 933.
21 P.S. Braterman, R.W. Harril and H.D. Kaesz, *J. Am. Chem. Soc., 89* (1967) 2851.
22 N. Flitcroft, D.K. Huggins and H.D. Kaesz, *Inorg. Chem., 3* (1964) 1123.
23 R.R. Andréa, W.G.J. de Lange, T. van der Graaf, M. Rijkhoff, D.J. Stufkens and A. Oskam, *Organometallics, 7* (1988) 1100.
24 G.J. Stor, J.W.M. van Outersterp, F. Hartl and D.J. Stufkens, to be published.
25 D.J. Cox and R. Davis, *J. Organomet. Chem., 186* (1980) 339.
26 N. Flitcroft, J.M. Leach and F.J. Hopton, *J. Inorg. Nucl. Chem., 32* (1970) 137.
27 J.E. Ellis and E.A. Flom, *J. Organomet. Chem., 99* (1975) 263.
28 M.L. Ziegler, H. Haas and R.K. Sheline, *Chem. Ber., 98* (1965) 2454.
29 H.K. van Dijk, J. van der Haar, D.J. Stufkens and A. Oskam, *Inorg. Chem., 28* (1989) 75.
30 G.W. Harris, J.C.A. Boeyens and N.J. Coville, *J. Chem. Soc., Dalton Trans.,* (1985) 2287.